RSC Advances

PAPER

View Article Online
View Journal | View Issue

Cite this: *RSC Adv.*, 2022, **12**, 6649

Flexible thermal conductive Al_2O_3@siloxane composite with rapid self-healing property based on carboxyl-amine dynamic reversible bonds†

Ziyue Hu, Weijian Wu, Xiang Chen,* Yuanzhou Chen, Junlin Chen and Zhifeng Hao*

Thermal interface materials (TIMs) are one of the efficacious ways to alleviate the heat accumulation problem of microelectronics devices. However, conventional TIMs based on polydimethylsiloxane (PDMS) always suffer from mechanical damage, leading to shortened service life or loss of thermal conductivity. In this work, we fabricated a high-thermal conductivity and fast self-healable Al_2O_3@siloxane composite by hydrosilylation reaction. The siloxane matrix consisted of thermosetting silicone rubber matrix (SR) and heat reversibility matrix (SCNR); the SR was synthesized *via* hydrosilylation between silicon hydrogen bond and vinyl, the SCNR was fabricated by thermal-curing between amino and carboxyl functionalized PDMS. Different sized spherical Al_2O_3 fillers were introduced into the SR/SCNR matrix system to construct the Al_2O_3@SR/SCNR composites. By adjusting the ratio of SR/SCNR, the obtained composites can achieve flexibility, self-healing and high filling simultaneously. It is notable that the self-healing efficiency of the composite is high, up to 95.6% within 3 minutes with 6.7 wt% mass ratio of SCNR/SR; these fast self-healing behaviors benefit from the assistance of thermal diffusion by 3D heat conduction pathways on the rearrangement of the dynamic cross-linked network. The resultant composites also exhibited the optimal thermal conductivity of 5.85 W mK^{-1}. This work provides a novel approach for constructing longer service life and high thermal conductivity multifunctional TIM based PDMS.

Received 26th December 2021
Accepted 21st February 2022

DOI: 10.1039/d1ra09367c

rsc.li/rsc-advances

Introduction

With the increasing refinement of the internal layout of microelectronic devices, heat is further accumulated. The electronics industry urgently desires to develop low-cost thermal interface materials (TIMs) which are suitable for irregular gaps to dissipate heat quickly.[1–3] Polydimethylsiloxane (PDMS) is widely used in the matrix of a new generation of TIMs due to its chemical stability and weather resistance.[4,5] However, the thermal conductivity of PDMS is only about 0.2 W mK^{-1}, so it is often necessary to fill with thermal conductive fillers to increase the thermal conductivity. Metal materials such as Ag,[6,7] Cu [8] and carbon materials including graphite,[9,10] graphene,[11,12] carbon nanotubes[13,14] with high electrical conductivity have been reported as fillers to increase the thermal conductivity of the polymer-composites. Ceramic materials such as AlN,[15] BN,[16,17] Al_2O_3 [18,19] have not only good thermal conductivity, but also good electrical insulation and excellent thermal stability. Among them, although the thermal conductivity of Al_2O_3 is not so high (~30 W mK^{-1}), it is widely sourced, inexpensive and suitable for bulk filling. It is applied in currently commercialized TIMs (such as thermally conductive gaskets and thermally conductive gels) to improve the thermal conductivity.

However, the conventional thermosetting Al_2O_3/PDMS composites are easily damaged to occur cracks during use, and thermal conductivity or other functions of the materials will be reduced after damage. The concept of self-healing comes from the healing process of natural organisms. Materials can maintain their properties after self-healing. If these TIMs are integrated with self-healing ability to automatically repair damages inflicted on them, it would avail long-term usage as well as enhanced reliability and durability. The intrinsic self-healing ability of materials is mainly achieved by dynamic reversible bonds, such as disulfide bonds,[20,21] Diels–Alder reactions,[22,23] amide bonds,[24,25] metal ligand-coordination,[26,27] borate bonds,[28,29] borate ester bond,[30,31] electrostatic interactions[32,33] and so on. Considering the practical application of thermal interface, the introduction of thermally triggered reversible dynamic bond is a suitable scheme. Whereas, among reported self-healing materials with thermally triggered reversible dynamic bond, Cao *et al.* fabricated a mechanically strong and self-healing rubbers *via* dynamic Fe^{3+}–pyridine coordination bonds, the sample shown self-healing efficiency of 87%.[34] Whereas, such metal coordination bonds are not suitable for

Guangdong Provincial Key Laboratory of Plant Resources Biorefinery, School of Chemical Engineering and Light Industry, Guangdong University of Technology, Guangzhou 510006, China. E-mail: chenxiang@gdut.edu.cn; haozf@gdut.edu.cn

† Electronic supplementary information (ESI) available. See DOI: 10.1039/d1ra09367c

occasions where insulation is required. Zhao *et al.* prepared the composite with thermal conductivity of 0.8 W mK^{-1} using DA adduct cross-linked silicone polymer as matrix and BN as fillers.[35] Therefore, achieving high thermal conductivity and fast self-healing efficiency is still a challenge. In particular, the materials should remain flexible.

It is an ingenious strategy to meet the demand introducing of the thermal-triggered carboxyl-amine dynamic bond into the siloxane matrix. Liu *et al.* fabricated a self-healing silicone elastomer *via* thermo-curing to develop dynamic crosslinked ionic bonds between carboxyl and amide functionalized PDMS, which showed a self-healing efficiency of 97% after 2 h, at 100 °C.[33] Sun *et al.* prepared a supramolecular network by two components assembled by hydrogen and ionic bonds, which a self-healing efficiency of 115% in tensile strength and almost 100% in actuated strain at a given electric field can be achieved after self-healing at 80 °C for 5 h.[32]

Inspired by the above works, we developed fast self-healing and high thermally conductive Al_2O_3@SR/SCNR composite based on carboxyl-amine dynamic reversible crosslinking. To meet the soft and high filling requirements of TIMs, we constructed a thermosetting silicone rubber matrix (SR) with low cross-linking degree *via* controlled hydrosilylation. The dynamic cross-linking network of SCNR formed between carboxyl and amide functionalized PDMS ensured self-healing and reprocessing capabilities. The spherical Al_2O_3, as a thermal conductive candidate, could make great contribution not only to fast heat pathway but also to the thermal-triggered self-healing properties. In addition, we adjusted the ratio of covalent crosslinks and thermo-reversible crosslinks in matrix to obtain both the fast self-healing performance and high thermal conductivity. It is reasonably expected that these multifunctional Al_2O_3@SR/SCNR composites would be used as preferable thermal interface materials which behave the ability to automatically repair damages and avail long-term usage as well as enhanced reliability and durability.

Experimental

Materials

Polyvinylsiloxane (PDMS-Vi) (RH-Vi311, Vi wt% = 0.43%), hydrogen siloxane (PDMS-H) (RH-H57, H wt% = 0.13%; RH-H512, H wt% = 1.2%; RH-H45, H wt% = 0.12%), Zhejiang Runhe Organic Silicon New Material Co., Ltd. (Huzhou China); lithium hydroxide, 1,3-2 vinyl-1,3,3,3-tetramethyldisiloxane platinum, 2-phenyl-3-butyn-2-ol, toluene, tetrahydrofuran (THF) methyl methacrylate (MMA), Aladdin Biochemical Technology Co., Ltd (Shanghai China) amino functionalized polydimethylsiloxane (PDMS-NH_2), Changji Chemical Co., Ltd. (Changshu China); spherical Al_2O_3 powders (20–70 μm), Foshan Sanshui Jinge New Material Co., Ltd.

Preparation of ester modified PDMS (PDMS-MMA)

10.0 g RH-H512 was dissolved into 30 mL toluene in a 250 mL three neck round bottom flask with a condensation reflux device and a dropping funnel, and a toluene (30 mL) solution containing 14.4 g of MMA was added slowly through a dropping funnel, and the reactants were stirred and dissolved in N_2 atmosphere, then 0.1 mL 1,3-2 vinyl-1,3,3, 3-tetramethyldisiloxane platinum was added into flask. After stirring for 15 min, reacting at 85 °C for 10 h, toluene and residual MMA were removed by distillation under reduced pressure to obtain a milky white viscous liquid PDMS-MMA (Fig. S1†).

Preparation of carboxyl functionalized PDMS (PDMS-COOH)

22.0 g PDMS-MMA was dissolved completely in 60 mL THF in a 500 mL single-neck round bottom flask, 145 mL of 1 mol L^{-1} LiOH aqueous solution was added slowly and condensed and refluxed for hydrolysis at 90 °C for 1 h. After the hydrolysis reaction is end, the aqueous phase was collected and then extracted in 40 mL THF at room temperature, the pH was adjusted to 1–2 with hydrochloric acid of 6 mol L^{-1}. The THF phase was collected, and the solvent was removed by distillation under reduced pressure to obtain a pale-yellow liquid PDMS-COOH (Fig. S1†).

Preparation of SCNR elastomer

PDMS-COOH and PDMS-NH_2 (molar ratio 1 : 1) were mixed uniformly in 50 mL THF for 3 h, the solvent was removed, the remaining solvent was volatilized at room temperature, and it was placed in a vacuum drying oven at 75 °C for 48 h to obtain SCNR elastomer (Fig. S1†).

Fabrication of Al_2O_3@SR/SCNR composites

5.0 g RH-Vi311, 0.3133 g RH-H45, 0.1342 g RH-H57 and 0.05 g 2-phenyl-3-butyn-2-ol were mixed at 65 °C for 15 min, then chopped SCNR particles and spherical Al_2O_3 fillers were added in small amounts and several times, the mixture was stirred and mixed evenly at 90 °C for 1 h. 20 μL 1,3-2 vinyl-1,3,3, 3-tetramethyldisiloxane platinum was added and mixed at room temperature, degassed under vacuum for 30 minutes, and cured at 100 °C for 20 min (Fig. 1). The Al_2O_3@SR/SCNR composites were obtained. The samples in this study were marked according to the following format: mass ratio $(x : y : z) : x$ Al_2O_3 fillers@y SR matrix/z SCNR matrix. The contrast samples without SCNR were marked as: mass ratio $(x : 1) : x$ Al_2O_3@SR.

Characterization

Fourier transform infrared (FTIR) spectra were obtained on a Thermofisher IS50R. Nuclear magnetic resonance (^{1}HNMR) spectra were recorded on a Bruker Advanced III HD 400 MHz NMR spectrometer with $CDCl_3$ as the solvent. X-ray diffraction (XRD) experiments were test on Malvern Panalytical Aries with Cu Kα radiation at 15 kV and 40 mA. The morphological structures were detected with a Phenomworld Prox microscope for scanning electron microscopy (SEM). The rheological properties were tested on Anton Par rotary rheometer MCR301 with a 25 mm stainless steel parallel plate. The angular frequency range was set to 100–0.1 rad s^{-1} and 0.1% strain was applied in frequency sweep mode. A heating rate of 1 °C s^{-1}, a frequency of 1 Hz and strain of 0.5% were applied in temperature sweep

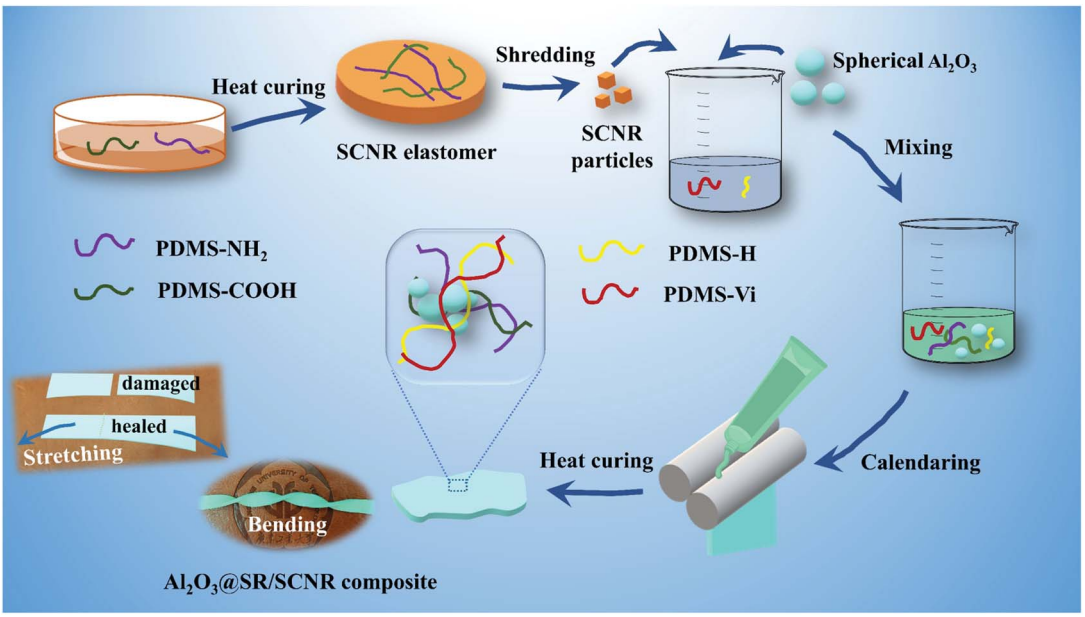

Fig. 1 Schematic diagram of fabrication of Al_2O_3@SR/SCNR composites.

mode. Differential scanning colorimetry (DSC) was conducted with a Mettler DSC3 by heating from −80 °C to 20 °C at a heating rate of 10 °C min^{-1} under nitrogen atmosphere. Thermal conductivity coefficients of samples were measured using a Netzsch LFA 467 light flash system at 25 °C, 260 V laser voltage, 0.6 ms laser pulse width, sampling frequency of 2 MHz, laser source of xenon lamp. Thermal conductivity (λ) coefficient is calculated from the follow formula:

$$\lambda = a \times \rho \times C_p$$

where α is the thermal diffusivity of the composite, ρ is the density of the composite with $\rho = m/v$, in which m and v are the mass and volume of the composites, respectively. C_p is the specific heat capacity which is obtained by DSC at 25 °C. The thermal date of samples was captured by a Magnity MAG12 infrared camera. Stress–strain curves of composite were determined on a IDEAR TEST electronic universal testing machine with 5 splines with the test rate of 100 mm min^{-1} at room temperature according to GB/T-528-2009. The self-healing efficiency of composites was calculated and evaluated from the ratio of the tensile strength of the healed samples to that of the original samples.

Results and discussion

The method and strategy of fabrication Al_2O_3@SR/SCNR composites

SCNR elastomer was prepared by blending PDMS-COOH and PDMS-NH_2, as shown in Fig. S1.† PDMS-COOH was prepared by hydrosilylation of side chain hydrogen polydimethylsiloxane (PDMS-H, H wt% = 1.2%) and MMA. Then, the synthesized PDMS-COOH was mixed with PDMS-NH_2 *via* solution blending. After removing the solvent and thermal curing, SCNR can be successfully obtained. The ionic bonds can be formed between PDMS-COO^- and PDMS-NH_3^+, which are generated by the deprotonation of –COOH on the side chain of PDMS-COOH and the protonation of –NH_2 at the end of PDMS-NH_2. In addition, hydrogen bonds can also be formed between carbonyl (C═O) and amino (NH_2). Carbonyl as a receptor, amine as a donor hydrogen bond and ion bond can be used as physical crosslinking points to form an elastomer network.

Al_2O_3@SR/SCNR composite was fabricated with blending and crosslinking SCNR particles, Al_2O_3, PDMS-Vi and PDMS-H. It is found that the free amino group destructed the reaction between PDMS-Vi and PDMS-H, so the PDMS-COOH in this system is slightly excessive and SCNR needs to be cured in advance. Under the pression, the added components crosslinked together uniformly to obtain Al_2O_3@SR/SCNR composites. It can be seen in Fig. 2(b) that there are no larger particles (such as SCNR) in the Al_2O_3@SR composites than the spherical alumina (20–70 μm). The low-crosslinking network we designed in this work can accommodate 10 times more alumina than itself. The amount of alumina added reaches 90.9 wt%, and a large amount of spherical alumina builds thermal conduction paths in all directions. And the successful preparation of Al_2O_3@SR/SCNR composites implied that SCNR is not recombined during the preparation. SR and SCNR networks are physically interspersed with each other. Moreover, SCNR particles were uniformly fused and inserted into SR network after continuous friction of Al_2O_3. Meanwhile, the permanently crosslinked SR network also acted as a skeleton to accommodate Al_2O_3 and SCNR networks.

Characterization and dynamic reversibility of the SCNR composites

SCNR is obtained *via* thermal-crosslinking of PDMS-COOH and PDMS-NH_2 (Fig. S1†), which the dynamic ionic bond formed between PDMS-COO^- and PDMS-NH_3^+. FTIR spectra for PDMS-

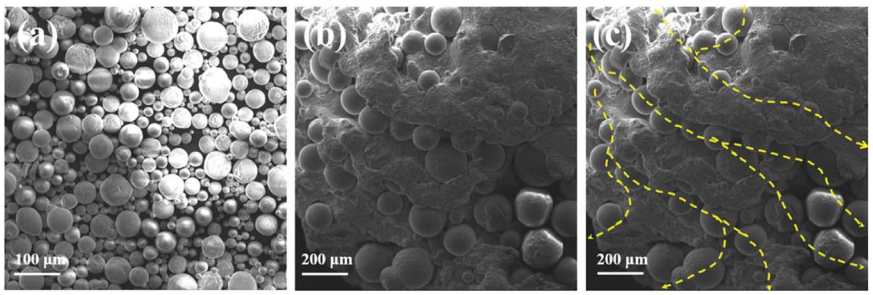

Fig. 2 SEM images of spherical alumina (a); Al_2O_3@SR/SCNR composites (b); thermal path of Al_2O_3@SR/SCNR composites (c).

H, PDMS-MMA, PDMS-COOH were present in Fig. S3(a).† PDMS-H has an obvious Si–H absorption at 2159 cm^{-1}. For PDMS-MMA, the absorption of Si–H basically disappeared, and a strong absorption of saturated ester carbonyl C=O appeared at 1743 cm^{-1}, indicating that a hydrosilylation reaction had occurred between MMA and PDMS-H. The main change in the FTIR spectrum of the product PDMS-COOH after the hydrolysis reaction was the disappearance of the absorption of the ester carbonyl C=O at 1743 cm^{-1} and the appearance of the absorption of the carboxyl group C=O at 1708 cm^{-1}. This confirmed that the ester functional group grafted onto the siloxane chain is successful hydrolysis to be a carboxyl functional group.

^{1}HNMR results (Fig. S2†) of PDMS-MMA ^{1}HNMR (400 MHz, $CDCl_3$) δ 7.15 (dd, J = 9.3, 5.5 Hz, 1H), 7.09–7.02 (m, 1H), 3.54 (s, 3H), 2.25 (s, 1H), 1.10 (d, J = 7.0) and PDMS-COOH (^{1}H NMR (400 MHz, DMSO-d_6) δ 11.91 (s, 1H), 1.74–1.61 (m, 1H), 0.68–0.44 (m, 1H)) also agree well with the FTIR data.

To illustrate the self-healing property of SCNR, the samples were cut into two different colour separate pieces with a razor blade (Fig. 3(a)), and two half-plates were brought back into contact and then healed by a thermal treatment at 90 °C, 1 h. The healed SCNR could be stretched and bent, indicating that the cured sample had good uniformity, and the chopped SCNR (Fig. 3(b)) could be reprocessed after hot pressing at 2 kPa, 90 °C for 15 min.

In situ FTIR was performed to study dynamic reversibility and the hydrogen bonds and ionic bonds network of SCNR. The infrared spectrum from 1500 cm^{-1} to 1800 cm^{-1} was presented in Fig. 4. Herein, in SCNR, hydrogen bonds were mainly formed among amide bond (N–H) and carbonyl (C=O) groups. As the peak representing stretching vibration of (C=O) groups moved

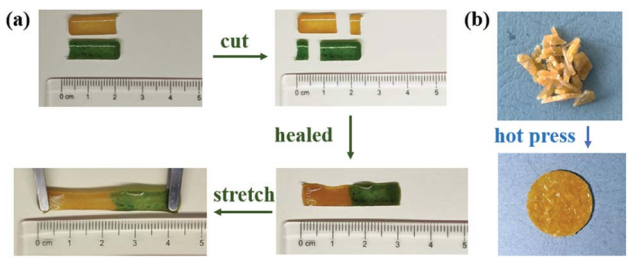

Fig. 3 Photographs of the SCNR: (a) self-healing of damaged SCNR samples; (b) reprocessing of SCNR samples.

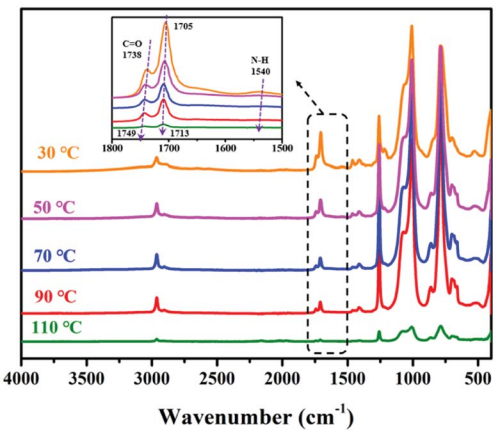

Fig. 4 *In situ* FTIR spectra of SCNR at different temperature.

from 1738 cm^{-1} to the high frequency region to 1749 cm^{-1}, accompanied with the shifting peak of in-plane bending vibration of N–H at 1540 cm^{-1} gradually to the low frequency region and disappeared. It could be inferred that hydrogen bonds interact with each other and the dynamic change of hydrogen bonds in the SCNR.[36] And the N–H peak disappears and the C=O peak weakens, which indicates that with the increase of temperature, the dynamic interaction decreases until dissociation, resulting in an increase in the amount of free carboxyl, thereby promoting the reaction of –COOH with –NH_2 to form carboxyl-amine dynamic bonds.

X-ray diffraction (XRD) patterns of SCNR before and after self-healed exhibited in Fig. S3(b).† The SCNR sample had no obvious crystallization peak, while the sample after heat treatment had a significant peak at about 45°, which may be explained by the fact that some hydrogen bonds are converted into ionic bonds after heat treatment, resulting in higher crystallinity, which is accordant with the results from *in situ* FTIR.

Flexible performance of the Al_2O_3@SR/SCNR composites

DSC studies chain mobility of Al_2O_3@SR/SCNR composites

Silicone elastomers are applied extensively because of their soft and elastic properties, especially the strong mobility of molecular chain plays a key role in self-healing materials.[37,38] The chain mobility of PDMS-COOH, SCNR elastomer, Al_2O_3@SR

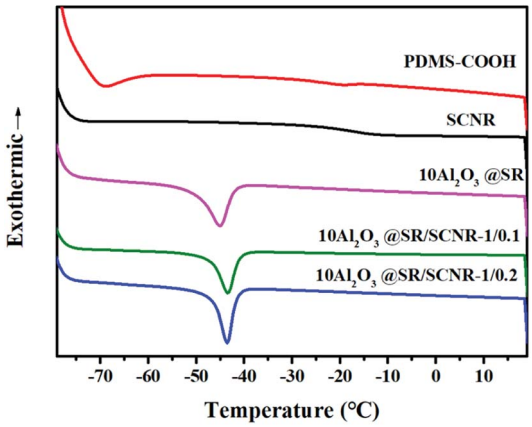

Fig. 5 DSC results of PDMS-COOH, SCNR, Al_2O_3@SR composites, Al_2O_3@SR/SCNR composites.

and Al_2O_3@SR/SCNR were measured by DSC in this work, as shown in the Fig. 5. The *Tg* of PDMS-COOH appears at −19 °C, while the T_g of SCNR is higher than −13 °C of PDMS-COOH, which is because the crosslinking limits the chain movement. The endothermic peak of Al_2O_3@SR at −45 °C corresponds to the melting of SR. The endothermic peak of Al_2O_3@SR/SCNR appeared at −43 °C, as the increasing of crosslinking SCNR limit the chain migration. Melting behaviour corroborates the softness and diffusivity in the composite, promoting the self-healing behavior.[39]

Rheological studies of the Al_2O_3@SR/SCNR composites

The rheological test is used to further investigate the elasticity and dynamic ionic crosslinking of composites. As shown in the frequency sweep test of Fig. 6(a) and (b), the storage modulus (G'') of the Al_2O_3@SR composites was always larger than the loss modulus (G') over the entire range of frequencies and exceed G'' by an order of magnitude, suggesting that the Al_2O_3@SR composites are solid elastomers. And the G'' improved with the increasing of the fillers loading, which was due to the reinforcement of the fillers that enhances the composites. The reason for G' increasement is that the increase of the fillers enlarges the friction between the fillers and the silicone molecular chain.

In the temperature scan test, as shown in Fig. 6(c) and (d), the Al_2O_3 loading is the same. The results show that the G'' of the composites are always higher than the G', demonstrating that the Al_2O_3@SR/SCNR composites are elastic solids in the temperature range of 20 °C to 140 °C. With the SCNR content increasing, and the G'' and G' of the Al_2O_3@SR/SCNR composites reduced, it might be explained by the fact that the binding force of dynamic reversible cross-linked ionic bonds of SCNR is weaker than that of permanent cross-linked covalent bonds of SR. In addition, as the SCNR wt% increases, the G'' and G'

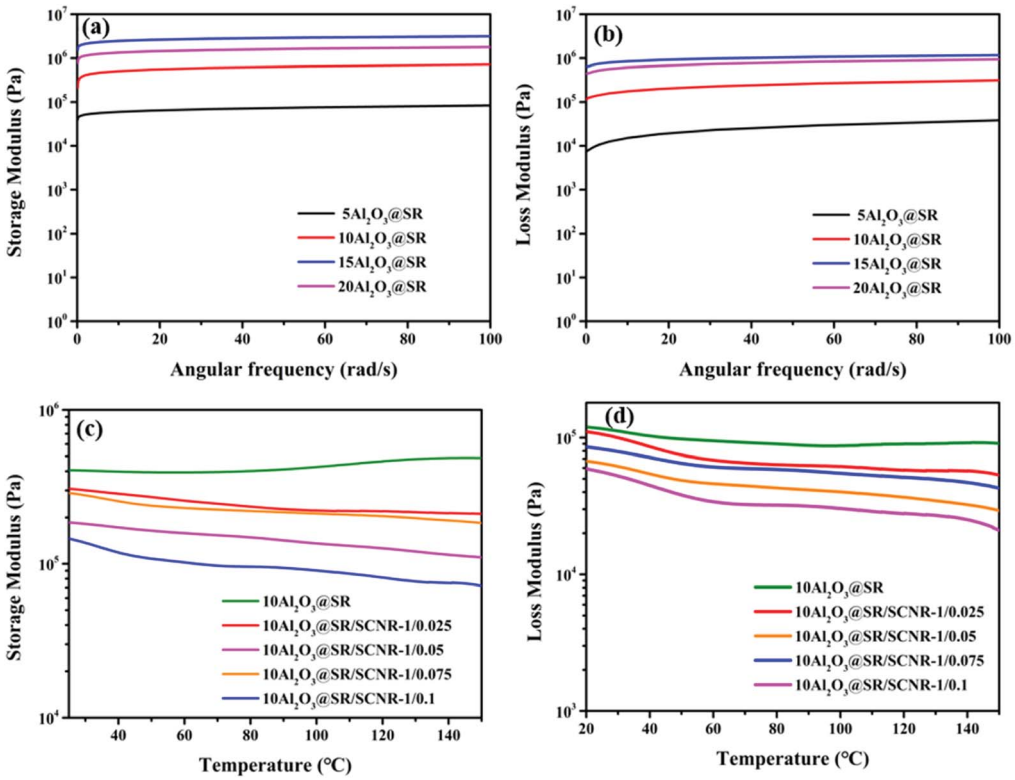

Fig. 6 In the frequency sweep test: (a) G'' of Al_2O_3@SR composites filled with different Al_2O_3 content; (b) G' of Al_2O_3@SR composites filled with different Al_2O_3 content; in the temperature scan test: (c) G'' of Al_2O_3@SR/SCNR composites with different SCNR content; (d) G'' of Al_2O_3@SR/SCNR composites with different SCNR content.

reduced, while G'' of Al_2O_3@SR does not enhance as the temperature rising. The phenomenon of decline occurred due to SR matrix was entirely composed of permanently cross-linked covalent bonds and will not dissociate with the increase of temperature. G'' of Al_2O_3@SR/SCNR composites exhibited a downward trend as the temperature increases. This was because the dynamic reversible ionic reaction of carboxyl and amino groups. The ionic bond dissociated gradually with the rise of temperature, leading to the loose crosslinking network and the decrease of G''.[32]

Self-healing performance of the Al_2O_3@SR/SCNR composites

Mechanical properties reversibility of the composites

The self-healing property of the Al_2O_3@SR/SCNR composites were valued *via* comparing the tensile strengths of the samples before and after healed at 2 kPa, 90 °C for 3 min. Fig. 7(a) exhibited the stress–strain curve of $10Al_2O_3$@SR/SCNR composites with different SCNR content. The value of elongation at break mainly depends on the ratio between SR and SCNR, SR has a smaller G'' compared to SCNR, and thus has elongation at breakage. As the SCNR content increases, the tensile strength of the composites increased obviously but the elongation decreased, it could be explained by the increase of crosslinking points in the system, and the degree of entanglement between the SCNR network and SR networks enhanced, and friction between fillers and chain grew up, restricting the free movement of the molecular chains, so the tensile strength increased. In addition, the reduction of elongation may be owing to weaker ionic bonds are easier to be broken before the permanent covalent bonds in SR.

Moreover, amount of converted ionic bonds in the composite after self-healed grew as the SCNR content increased, so the tensile strength grew up, it probably leaded to a stronger composite which may sustain the repeated stress and prolong the service life until next breakdown.

Fig. S5† shown the stress–strain curves of the original and the self-healed Al_2O_3@SR/SCNR composites with different SCNR content. The data of healing efficiency of the Al_2O_3@SR/SCNR composites was listed in Table 1. It is worth noting that Al_2O_3@SR/SCNR could self-healed after hot press treatment, but Al_2O_3@SR did not show self-healing properties. The $10Al_2O_3$@SR/SCNR-1/0.075 behaved the best self-healing efficiency up to 98.38%, and the self-healing efficiency of $20Al_2O_3$@SR/SCNR-1/0.075 was 95.6%, which SCNR content of matrix was just 6.97 wt%. The results indicated that the introduction of SCNR endowed with self-healing property. The high self-healing efficiency is also on account of the flexibility of the silicone macromolecular chain. Otherwise, when the addition of SCNR exceeded 6.97 wt%, the viscosity of the system was too large and restricted the self-healing efficiency. This was due to the increase of cross-linking point, the degree of friction with the filler increases, and the resistance of molecular chain migration increased. The thermal rearrangement of carboxyl amine dynamic bond was difficult to migrate and contact, leading to the self-healing performance decreased. Therefore, the ratio between SR and SCNR was critical for efficient self-healing properties of composites.

A numerical contrast of the thermal conductivity, self-healing efficiency and the time on self-healing of the as-fabricated Al_2O_3@SR/SCNR composites with other thermal conductivity, self-healing composites[35,40–46] reported previously are displayed in Table S2† and Fig. 7(b). It was significant that the Al_2O_3@SR/SCNR composites in this work exhibited excellent comprehensive performance compared to other self-healing TIMs and demonstrated hopeful application potential in the field of microelectronics.

Thermal conductivity reversibility of the composites

The thermal conductivity (λ) of Al_2O_3@SR composites and Al_2O_3@SR/SCNR composites before and after self-healed were tested *via* laser flash method. The ratio of Al_2O_3/SR/SCNR in Al_2O_3@SR/SCNR composites was x/1/0.075, the ratio of Al_2O_3/SR in Al_2O_3@SR composites was y/1. The calculated λ was displayed in Fig. 8, as the content of Al_2O_3 increased, the λ of both Al_2O_3@SR and Al_2O_3@SR/SCNR composites increased. Fig. 8(a) revealed that the λ of the $20Al_2O_3$@SR/SCNR-1/0.075 is 5.86 W

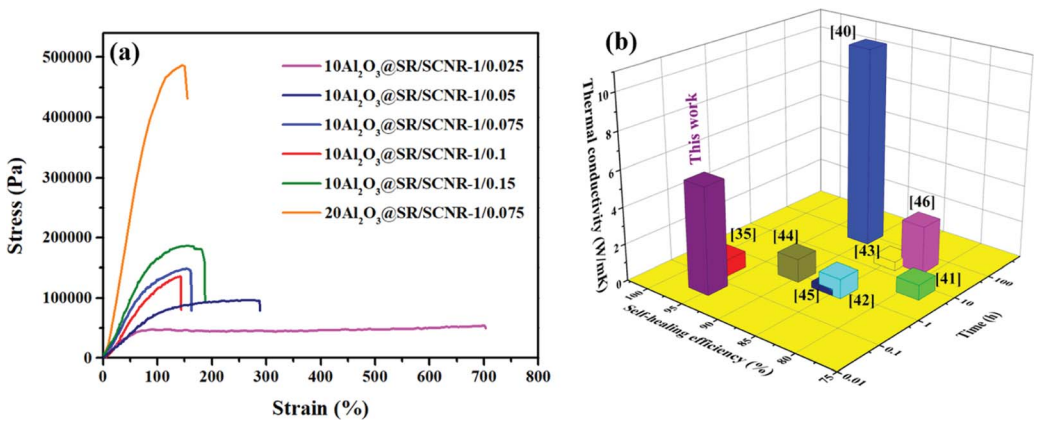

Fig. 7 (a): Stress–strain curve of Al_2O_3@SR/SCNR composites; (b) the comparison of time on healing, thermal conductivity and self-healing efficiency between $20Al_2O_3$@SR/SCNR-1/0.75 and previously reported works.

Table 1 The data of healing efficiency of the Al_2O_3@SR/SCNR composites

Sample	Original tensile strength (MPa)	Original elongation at break (%)	Healed tensile strength (MPa)	Healed elongation at break (%)	Self-healing efficiency (%)
10Al_2O_3@SR/SCNR-1/0.025	0.053	701.439	0.043	498.564	82.02
10Al_2O_3@SR/SCNR-1/0.05	0.093	211.771	0.084	133.611	90.38
10Al_2O_3@SR/SCNR-1/0.075	0.147	187.305	0.145	157.464	98.13
10Al_2O_3@SR/SCNR-1/0.1	0.135	142.757	0.122	126.119	90.97
10Al_2O_3@SR/SCNR-1/0.15	0.198	172.772	0.164	152.600	82.87
20Al_2O_3@SR/SCNR-1/0.075	0.485	146.211	0.412	139.777	95.60

mK^{-1}, while the 20Al_2O_3@SR is 5.85 W mK^{-1} in Fig. 8(b), implying that the introduction of SCNR had little effect on the thermal conductivity.

In this work, Agari's model could predict the thermal conductivity of the material well when the fillers are in contact with each other and agglomerate to form a thermally conductive chain under high filling conditions. Formula as follows:

$$\lambda = \left(C_1\lambda_p\right)^{\left(1-V_f\right)}\lambda_{f2}{}^{C_2V_f}$$

Here, C_1 represents the influencing factor of the crystallinity and crystal size of the polymer, C_2 is the degree of difficulty in forming the thermal chain. According to the result of theoretical calculation and analysis illustrate in Fig. S8(a)†: $C_1 = 0.302$, $C_2 = 0.848$, indicated that it is easy to form a thermally conductive chains in the composites, and crystallinity and crystal size have little effect on thermally conductivity.

However, λ of 20Al_2O_3@SR/SCNR and 20Al_2O_3@SR before and after self-healed exhibited significant differences. Fig. 8(b) displayed that the Al_2O_3@SR composites without self-healing ability have worse thermal conductivity after damaged, the λ of 20Al_2O_3@SR was 4.95 W mK^{-1}, 13.4% drop than the original sample, the λ of 15Al_2O_3@SR also reduced 26.7%. Owing to no reversible bonds in Al_2O_3@SR, so slight damage causes partial heat conduction path interruption, which reduces the heat conduction performance and cannot be restored.

In contrast, the λ of 15Al_2O_3@SR/SCNR changed a little before and after self-healed from 3.395 W mK^{-1} to 3.39 W mK^{-1}. As for 20 Al_2O_3@SR/SCNR, it changed from 5.86 W mK^{-1} to 5.855 W mK^{-1}. The thermal conductivity of the Al_2O_3@SR/SCNR composites can be recovered as high as 99.8% after hot pressing treatment. As shown in the Fig. 9(b), when Al_2O_3@SR/SCNR composites are damaged, the ionic crosslinking on the fracture surface can be reversibly dissociated and reconstructed, so that the damage can be repaired well. Furthermore, the pressure was applied to overcome the barrier of fillers to molecular chain migration, so that the molecular chain at the wound could in contact with each other, and the heat was quickly gathered at the wound through the 3D heat conduction pathways (Fig. 2(c)), so as to realize the rapid reconstruction of dynamic construction. And all the Al_2O_3@SR/SCNR composites were able to restore after hot pressing treatment as illustrated in Fig. S6,† which is recycle and meaningful for the sustainable development.

The TG and DTG curves in Fig. S4† present that Al_2O_3@SR/SCNR composites have excellent thermostability. The data of thermal degradation characteristics were shown in Table S1.† When the content of SCNR wt% in the matrix increased from 0 to 16 wt%, the residual mass at 700 °C decreased slightly from 90.73% to 88.43% and the initial decomposition temperature ($T_{d5\%}$) of Al_2O_3@SR was 607 °C. With the increasing of SCNR content in silicone matrix, the $T_{d5\%}$ of Al_2O_3@SR/SCNR composites firstly increased and then decreased. Compared with the Al_2O_3@SR, the residual mass at high temperature decreased by about 1%, while when SCNR accounted for 6.98% of the matrix mass fraction, $T_{d5\%}$ and T_{dmax} increased slightly.

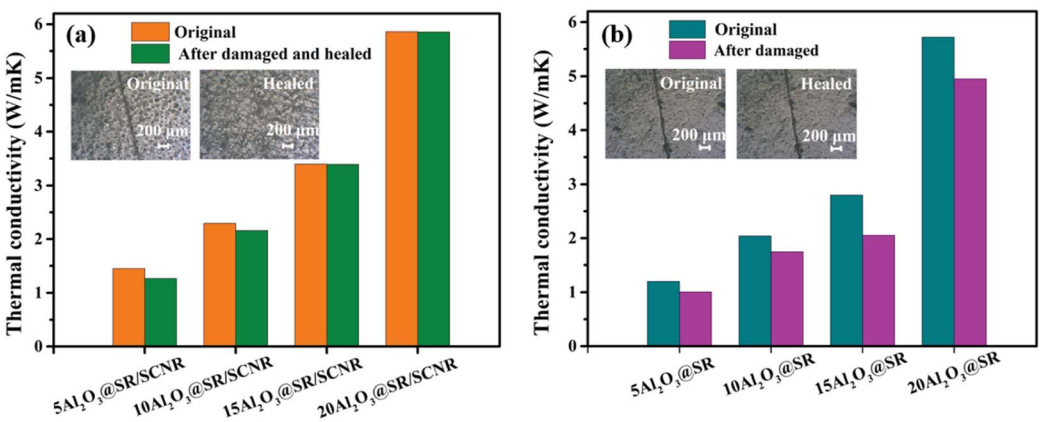

Fig. 8 (a) Thermal conductivity and microscopic images of the Al_2O_3@SR/SCNR composites before and after self-healed; (b) thermal conductivity and microscopic images of the Al_2O_3@SR composites before and after damaged.

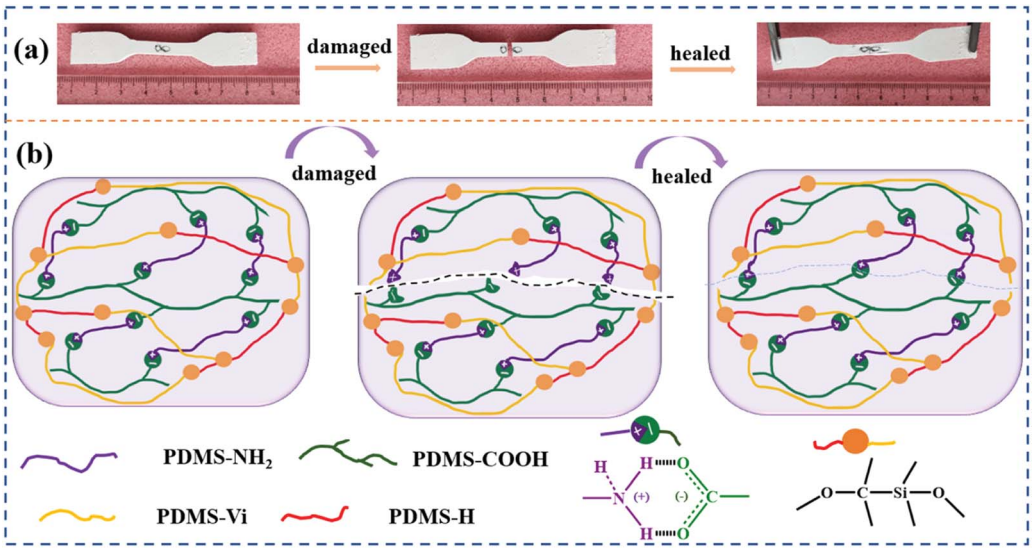

Fig. 9 (a) Photographs of self-healing performance of $10Al_2O_3$@SR/SCNR-1/0.075 composites; (b) schematic diagram of self-healing effect driven by dynamic reversibility of carboxyl-amine system.

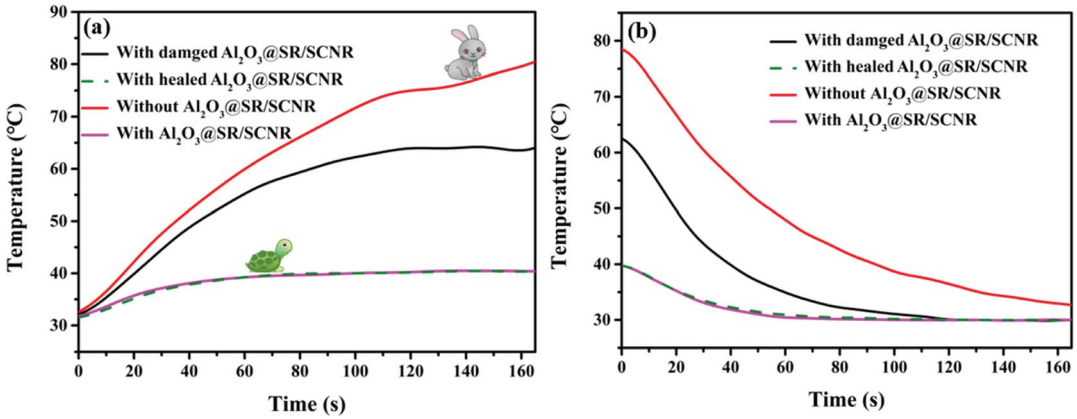

Fig. 10 (a) Temperature rise curves of blub on Al_2O_3@SR/SCNR before and after self-healed since power on; (b) cooling curves of blub on Al_2O_3@SR/SCNR before and after self-healed after power off.

The Al_2O_3@SR/SCNR composites showed excellent thermostability. This further ensured the reliability of the composites in high temperature applications.

Thermal management properties of the composites

Al_2O_3@SR/SCNR composites were installed on the working blub to test its actual heat dissipation ability in microelectronic devices. In Fig. 10(a), for the blub without Al_2O_3@SR/SCNR, the temperature of the blub rose rapidly to 73.03 °C within 100 s after power on, exceeding the safe temperature (60 °C) and then continuing to rise. Meanwhile, the temperature of the blub installed with $20Al_2O_3$@SR/SCNR only increased slightly to 40.06 °C, which was 46.31% lower than that of the single blub and remained in equilibrium, suggesting that heat dissipation speed of the Al_2O_3@SR/SCNR and the heating speed of the blub reached a balance, so the Al_2O_3@SR/SCNR behaved good heat dissipation capacity. In addition, for the blub installed of damaged Al_2O_3@SR/SCNR, the temperature rose to 60 °C, the heat dissipation capacity was significantly lower than the original, which was caused by mechanical damage. But the for the Al_2O_3@SR/SCNR after self-healed, its heat dissipation capacity almost recovered. Therefore, self-healing property is important for TIMs materials in practical use.

The cooling process after power off was shown in Fig. 10(b). The cooling rate of the blub with Al_2O_3@SR/SCNR is evidently faster than that of the individual blub, and the heat dissipation performance of the blub with the Al_2O_3@SR/SCNR was basically completely restored after self-healed. Therefore, the Al_2O_3@SR/SCNR after self-healed could efficiently self-repair internal damage and conduct the accumulated heat in time, and the heat dissipation rate was quickly.

Conclusions

In this work, we successfully fabricated fast self-healing and high thermally conductive Al_2O_3@SR/SCNR composites based

on carboxyl-amine dynamic reversible bonds. We used the dynamic and reversible cross-linking between the carboxyl and the amino functional PDMS to synthesize the SCNR with heat reversibility, then the different sizes spherical Al_2O_3 fillers and SCNR particles were introduced into the SR system to construct the Al_2O_3@SR/SCNR composites *via in situ* polymerization. The $20Al_2O_3$@SR/SCNR-1/0.075 composites with 6.97 wt% SCNR content of matrix exhibited the thermal conductivity of 5.89 W mK^{-1} and the self-healing efficiency up to 95.6% simultaneously. The dynamic ionic reaction between the carboxyl and the amino functionalized PDMS was considered to be the source of high-efficiency self-healing performance. The introduction of alumina improved the thermal conductivity of the composites and accelerated the speed of heat transfer. At the same time, the heat conduction pathway provided fast and uniform heat for the self-healing quickly of the damaged area, and $20Al_2O_3$@SR/SCNR composite behaved excellent heat dissipation performance in the field of microelectronics. The brief strategy in this work provides a practical method that can be used as a reference for other self-healing thermally conductive polymer thermal interface materials.

Conflicts of interest

There are no conflicts to declare of interest.

Acknowledgements

We greatly acknowledge the financial support from the Applied Science and Technology Research and Development Special Foundation of Guangdong Province (No. 2016 B0909 30004) and National Natural Science Foundation of China (No. 52150410401).

References

1 X. T. Yang, C. B. Liang, T. B. Ma, Y. Q. Guo, J. Kon, J. W. Gu, M. J. Chen and J. H. Zhu, *Adv. Compos. Hybrid Mater.*, 2018, **1**, 207–230.
2 C. P. Cheng, L. Y. Yang, J. Yang, L. Bai, R. Y. Bai, Z. Y. Liu, M. B. Yang, H. B. Yang and W. Yang, *Compos. Commun.*, 2020, **22**, 100528.
3 J. Khan, S. A. Momin and M. Mariatti, *Carbon*, 2020, **168**, 65–112.
4 Y. Meng, W. J. Xu, M. R. Newman, D. W. Benoit and M. Anthamatten, *Adv. Funct. Mater.*, 2019, **29**, 1903721.
5 E. Yilgor and I. Yilgor, *Prog. Polym. Sci.*, 2014, **39**, 1165–1195.
6 J. Kim, S. Lee, C. Kim, Y. Park, M. Kim and J. H. Seol, *Polymers*, 2020, **12**, 1805.
7 Y. J. Wu, X. X. Zhang, A. Negi, J. X. He, G. X. Hu, S. S. Tian and J. Liu, *Polymers*, 2020, **12**, 426.
8 P. K. Dhawan, M. Wan, A. Srivastava, V. Singh and R. R. Yadav, *J. Mater. Sci. Eng. B*, 2019, **249**, 114407.
9 C. Li, L. Y. Tan, X. L. Zeng, D. L. Zhu, R. Sun, J. B. Xu and C. P. Wang, *Compos. Sci. Technol.*, 2020, **188**, 107970.
10 A. S. Kurian, V. B. Mohan, H. Souri, J. S. Leng and D. Bhattacharyya, *J. Mater. Res. Technol.*, 2020, **9**, 15621–15630.
11 F. Jiang, X. L. Cui, N. Song, L. Y. Shi and P. Ding, *Compos. Commun.*, 2020, **20**, 100350.
12 S. Li, Y. Li, X. Han, X. R. Zhan and Y. Zhao, *Composites, Part A*, 2019, **120**, 95–105.
13 Y. Z. Chen, J. L. Chen, Y. M. Zhang, Z. Y. Hu, W. J. Wu, X. Chen and Z. F. Hao, *Nanomaterials*, 2021, **11**, 2504.
14 Y. Hu, S. W. Chiang, X. D. Chu, J. Li, L. Gan, Y. B. He, B. H. Li, F. Y. Kang and H. D. Du, *J. Mater. Sci.*, 2020, **55**, 9414–9424.
15 C. R Yang, C. D. Chen, C. Chen, W. H. Shi, P. H. Chen and T. P. Teng, *Int. J. Therm. Sci.*, 2020, **155**, 106431.
16 Y. Q. Guo, Z. Y. Lyu, X. Y. Yang, Y. J. Lu, K. P Ruan, Y. L. Wu, J. Kong and J. W. Gu, *Composites, Part B*, 2019, **164**, 732–739.
17 X. L. Chen, J. S. K. Lim, W. L. Yan, F. Guo, Y. N. Liang, H. Chen, A. Lambourne and X. Hu, *ACS Appl. Mater. Interfaces*, 2020, **12**, 16987–16996.
18 J. N. Song, Z. L. Peng and Y. Zhang, *Chem. Eng. J.*, 2020, **391**, 123467.
19 Y. F. Wen, C. Chen, Y. Z. Feng, Z. G. Xue, X. P. Zhou, X. L. Xie and Y. W. Mai, *Compos. Sci. Technol.*, 2020, **186**, 107971.
20 K. Li, Z. P. Xu, S. F. Zhao, X. Y. Meng, R. L. Zhang, J. H. Li, J. F. Leng, G. P. Zhang, D. X. Cao and R. Sun, *Chem. Eng. J.*, 2019, **371**, 203–212.
21 Y. L. Liu, J. G. Yuan, K. M. Zhang, K. Y. Guo, L. Yuan, Y. M. Wu and C. H. Gao, *Prog. Org. Coat.*, 2020, **144**, 105661.
22 C. C. Yang, D. D. Zhu, C. Y. Sun, B. Y. Chen, Y. H. Li, I. N. Pulidindi, Z. Zheng and X. L. Wang, *Compos. Sci. Technol.*, 2021, **208**, 108767.
23 D. Q. Li, S. Y. Wang, Y. J. Meng, Z. W. Guo, M. M Cheng and J. Li, *Carbohydr. Polym.*, 2021, **268**, 118224.
24 L. L. Cai, S. Liu, J. W. Gu and Y. G. Jia, *Acta Biomater.*, 2020, **113**, 84–100.
25 Y. Nurhamiyah, A. Amir, M. Finnegan, E. Themistou, M. Edirisinghe and B. Q. Chen, *ACS Appl. Mater. Interfaces*, 2021, **13**, 6720–6730.
26 J. C. Lai, L. Li, D. P. Wang, M. H. Zhang, S. R. Mo, X. Wang, K. Y. Zeng, C. H. Li, Q. Jiang, X. Z. You and J. L. Zuo, *Nat. Commun.*, 2018, **9**, 2725.
27 L. Z. Zhang, Z. H. Liu, X. L Wu, Q. B. Guan, S. Chen, L. J Sun, Y. F. Guo, S. L. Wang, J. C. Song, E. M. Jeffries, C. L. He, F. L. Qing, X. G. Bao and Z. W. You, *Adv. Mater.*, 2019, **31**, 1901402.
28 J. L. Cao, G. H. He, X. Q. Ning, C. Wang, L. H. Fan, Y. H. Yin and W. Q. Cai, *Int. J. Biol. Macromol.*, 2021, **174**, 89–100.
29 M. H. Liao, H. Liao, J. J. Ye, P. B Wan and L. Q. Zhang, *ACS Appl. Mater. Interfaces*, 2019, **11**, 47358–47364.
30 J. Y. Ai, J. B. Li, K. Li, F. Yu and J. Ma, *Chem. Eng. J.*, 2021, **408**, 127256.
31 H. Peng, Y. Y. Lv, G. G. Wei, J. Z. Zhou, X. J. Gao, K. J. Sun, G. F. Ma and Z. Q. Lei, *J. Power Sources*, 2019, **431**, 210–219.
32 H. B. Sun, X. Y Liu, S. T. Liu, B. Yu, N. Y. Ning, M. Tian and L. Q. Zhang, *Chem. Eng. J.*, 2020, **384**, 123242.
33 Z. Liu, P. Hong, Z. Y. Huang, T. Zhang, R. J. Xu, L. J. Chen, H. P. Xiang and X. X. Liu, *Chem. Eng. J.*, 2020, **384**, 123142.

34 L. M. Cao, Z. Gong, C. Liu, J. F. Fan and Y. K. Chen, *Compos. Sci. Technol.*, 2021, **207**, 108750.
35 L. W. Zhao, X. R. Shi, Y. Yin, B. Jiang and Y. D. Huang, *Compos. Sci. Technol.*, 2020, **186**, 107919.
36 X. P. Wang, D. Liang and B. K. Cheng, *Compos. Sci. Technol.*, 2020, **193**, 108127.
37 B. W. Li, J. H. Lan and L. Wang, *Phys. Rev. Lett.*, 2005, **95**, 104302.
38 M. Hernandez, M. M. Bernal, A. M. Grande, N. Zhong, S. van der Zwaag and S. J. Garcia, *Smart Mater. Struct.*, 2017, **26**, 85010.
39 Y. L. Chen, J. Tang, M. J. Kesler, Y. Y. Sham, R. Vince, R. J. Geraghty and Z. Q. Wang, *Bioorg. Med. Chem.*, 2012, **20**, 467–479.
40 H. T. Yu, Y. Y. Feng, C. Chen, Z. X. Zhang, Y. Cai, M. M. Qin and W. Feng, *Carbon*, 2021, **179**, 348–357.
41 H. T. Yu, Y. Y. Feng, L. Gao, C. Chen, Z. X. Zhang and W. Feng, *Macromolecules*, 2020, **53**, 7161–7170.
42 X. T. Yang, Y. Q. Guo, X. Luo, N. Zheng, N. Zheng, T. B. Ma, J. J. Tan, C. M. Li, Q. Y. Zhang and J. W. Gu, *Compos. Sci. Technol.*, 2018, **164**, 59–64.
43 D. W. Yue, H. Q. Wang, H. Q. Tao, P. Zheng, C. H. liu and J. L. Zuo, *Chin. J. Polym. Sci.*, 2021, **39**, 1328–1336.
44 X. T. Yang, X. Zhong, J. L. Zhang and J. W. Gu, *J. Mater. Sci. Technol.*, 2021, **68**, 209–215.
45 C. H. Jia, P. Zhang, S. M. Seraji, R. S. Xie, L. Chen, D. Liu, Y. Xiong, H. Chen, Y. K. Fu, H. L. Xu and P. A. Fu, *Composites, Part A*, 2022, **152**, 106686.
46 C. Chen, H. T. Yu, Y. Y. Feng and W. Feng, *Acta Polym. Sin.*, 2021, **52**, 272–280.